Materials and Structures (2023) 56:93
https://doi.org/10.1617/s11527-023-02182-0

ORIGINAL ARTICLE

Dowel behaviour of rebars under combined axial and shear actions

M. Preti · A. Paderno · L. Cominoli

Received: 9 June 2022 / Accepted: 27 April 2023 / Published online: 16 May 2023

Abstract The resource of shear resistance provided by the dowel mechanism of rebar in reinforced concrete (RC) structures can significantly affected by the simultaneous presence of axial loading. This occurs for example of plastic hinges of seismic resistant structures. In fact, at load reversals in cycles of large deformation demand, rebars are subjected to combined axial and shear loading, particularly in those section where the shear transfer via aggregate interlocking is jeopardized by the opening of the crack throughout the entire section depth. Thus, a reliable assessment of the shear capacity of dowels under combined shear and axial load is required to check the element shear resistance. The paper describes the results of a specific experimental campaign on rebar dowels subjected to shear loading in presence of different levels of axial load. Both smooth and ribbed rebar dowels were investigated. A marked reduction of the dowel shear strength and stiffness in presence of increasing axial loading was experimentally observed, only partially compensated by the kinking effect. The latter was found to characterize the entire resource of dowel capacity when the axial load was close to the rebar yielding strength. The paper proposes an analytical model, adapted from others available in the literature, to predict the dowel shear-displacement response accounting for the applied axial load. The model helps the understanding of the dowel response, is suitable for hand calculation and can easily assist the dowel design. The experimental response was quite well captured for smooth dowels, while the prediction was less accurate for ribbed ones. Future refinements may address the local damage induce by the rebar pull-out, typical of ribbed rebars, which is neglected in present form of the model.

Keywords Dowel action · Combined axial and shear action · Shear in plastic hinge · Reinforced concrete sliding shear · Analytical modeling · Dowel shear test

1 Introduction

The reinforced concrete (RC) structures under seismic action are typically designed to undergo large load and deformation demand at the frame member ends; significant crack opening is expected in those regions where plastic hinges occur and high plastic deformation demands are expected both on rebars and concrete. Cyclic actions reflect in shear and bending action inversion, therefore cracks crossing the element depth can be expected. The evaluation of shear transmission across a crack is a key aspect to assess the element capacity in transmitting lateral actions to

M. Preti (✉) · A. Paderno · L. Cominoli
Department of Civil, Environmental, Architectural Engineering and Mathematics, DICATAM, University of Brescia, Via Branze 43, 25123 Brescia, Italy
e-mail: marco.preti@unibs.it

adjacent members. When the crack orientation is orthogonal to the element axis, in absence of diagonal reinforcement, two main resisting mechanisms can be identified [1, 2]: concrete aggregate interlocking and dowel mechanism of crossing bars. The former is predominant in presence of significant normal contact stresses between the crack concrete faces. The high stiffness associated to an effective frictional mechanism prevents significant sliding on the crack plane; consequently, the dowel behaviour is basically inhibited and offers limited contribution to the lateral load resistance. However, the frictional mechanism can be jeopardized when the crack roughness deteriorates due to cyclic loading, in presence of tensile action or when high elongation demand on the tension rebars is not recovered at load reversals. Particularly at load reversal, some cracks may remain temporarily open before the axial load in the compressed rebar recovers the tensile inelastic elongation cumulated in the previous opposite loading during the cycle [3–6]. Thus axial, bending, and shear action may occur to be transferred through an opened crack. The issue characterizes the seismic response of RC members in presence of both ribbed and smooth rebars; in the first case a spread crack pattern is expected, whereas only few cracks open in members with plain reinforcement [7–9].

To mitigate the risk of sliding shear, codes often suggest providing inclined rebars at potential location of critical cracks, typically at the element ends and at the cold joints, but this option is not always convenient in practice. In the above presented scenarios, rebar dowel mechanism may result a key resource for the shear transfer across a cracked cross-section; however, since in a plastic hinge the same reinforcing bars are simultaneously subjected to axial stress, the understanding of the role of the axial load in the dowel mechanism capacity is necessary.

Several experimental tests and theoretical interpretation of bar dowel behaviour across a shear plane are available in the literature [10–21]. These works explicitly showed as the dowel mechanism is governed by the dowel bar bending resistance [12–14, 20]; thus, simultaneous axial load is expected to reduce the mechanism strength. Despite of that, limited experimental information can be found about the effects of a coupled action of axial and shear loading. Maekawa and Qureshi [17] focused on the effect of transversal imposed local displacement on the axial pull-out behaviour of a ribbed rebar, as due to a shear sliding at the crack location; the capacity resulted strongly influenced by the effect of the coupled action. Nevertheless, the specific test configuration did not allow to independently evaluate the shear and axial capacity of the rebar. Some relevant results are discussed by Matsunaga et al. [21], who tested the dowel response of straight rebar anchors under combined shear and axial load. The focus was on the role of the anchor slip, and the range of axial load explored was limited to 66% of rebar yielding stress. It is worth noting that the available tests focused mainly on response of deformed rebars, whose dowel response under axial load is significantly coupled with the damage of concrete surrounding the bar due to bar pull-out. In the knowledge of the authors, limited results [18] about the behaviour of smooth bars are available in literature, which are relevant as they are typical of a large building stock of existing RC frames [22, 23] realized in North America, New Zealand, and Mediterranean area in the period from the World War II to the Seventies.

The paper presents the results of an experimental campaign on the role of the axial stress acting on a rebar in its dowel mechanism capacity against shear sliding at about a crack. Focus is on the mechanism of dowel action of smooth rebars, which are slightly or negligibly affected by the concrete damage due to bond stresses in the mechanism of anchor pull-out. A range of axial stress from zero to 98% of the rebar yielding stress is explored. A total number of 20 specimens were tested, imposing a constant axial load and a cyclic shear loading on two pre-formed cracks crossed by a single bar. Only the ductile failure mechanism is investigated by inhibiting the possible concrete splitting phenomena [14] that may occur for example in precast construction or pavements connections; thus, specific sizing and confinement of the specimen sliding concrete blocks was chosen. The effect of damage due to rebar anchor bond in the concrete surrounding the dowel is also investigated by comparison with the response of the simpler smooth rebar mechanism. Dowel shear load–displacement response is analysed in terms of strength and stiffness, as a function of the axial stress in the rebar.

Finally, an analytical approach is defined to assess the dowel shear load versus displacement response under coupled axial and shear loads. The mechanism capacity in terms of strength and both initial and post

yielding stiffness are analytically defined with reference to mechanical concepts. Experimental and analytical results are then compared with some available formulations [16, 20, 24, 25] to discuss their efficiency in predicting the mechanism strength. The proposed model well captures the full load–displacement relationship for smooth bar dowels, while further development is needed to account for local concrete damage induced by the dowel pull-out as typical of ribbed rebars.

2 Experimental campaign

2.1 Specimen description and test set-up

The test was designed to apply a combined axial load and shear action on a single rebar as it may occur on a longitudinal rebar in reinforced concrete plastic hinges at an open crack. For experimental convenience, the dowel bar specimen is embedded in three aligned adjoining concrete blocks crossed by the rebar dowel (Fig. 1), separated each other by two pre-formed 3 mm gaps simulating two consecutive open cracks. Each concrete block has a 200 × 200 mm cross section and a 150 mm length. Such length was chosen with the following aims: (i) allow on both sides of the single gap an embedded length sufficiently large (more than three and a half times the dowel diameter in this case, according to [20, 26]) to ensure the development of the plastic hinge of the dowel mechanism (long embedment) inside the block; (ii) for the deformed rebar specimens, have the two gaps at a distance compatible with the crack spacing developing in plastic hinges of reinforced concrete structures, to allow for a plausible bond transfer in the central concrete block, as it occurs in between two subsequent flexural cracks in real elements; (iii) limit the specimens size and weight to optimize their workability. It is worth noting that for the smooth rebar specimens, the bond transfer is negligible, thus the condition (ii) does not apply to them; nonetheless, smooth rebar specimens were built with the same geometry and embedded length of the deformed rebar specimens to help the comparison of the results and for experimental efficiency. For smooth dowels, which represent rebars typically anchored with end restraints (bent or hook end), the axial load was applied directly to the dowel bar ends protruding from the external concrete prisms. In the case of ribbed dowels, in order to activate the bond stress transfer between the dowel bar and the surrounding concrete, the load was applied to the outer concrete prisms by means of four 12 mm treaded rod with an end bolt, casted in the prism near the corners and attached to the loading machine (Fig. 1b). A steel plate welded to the protruding bar

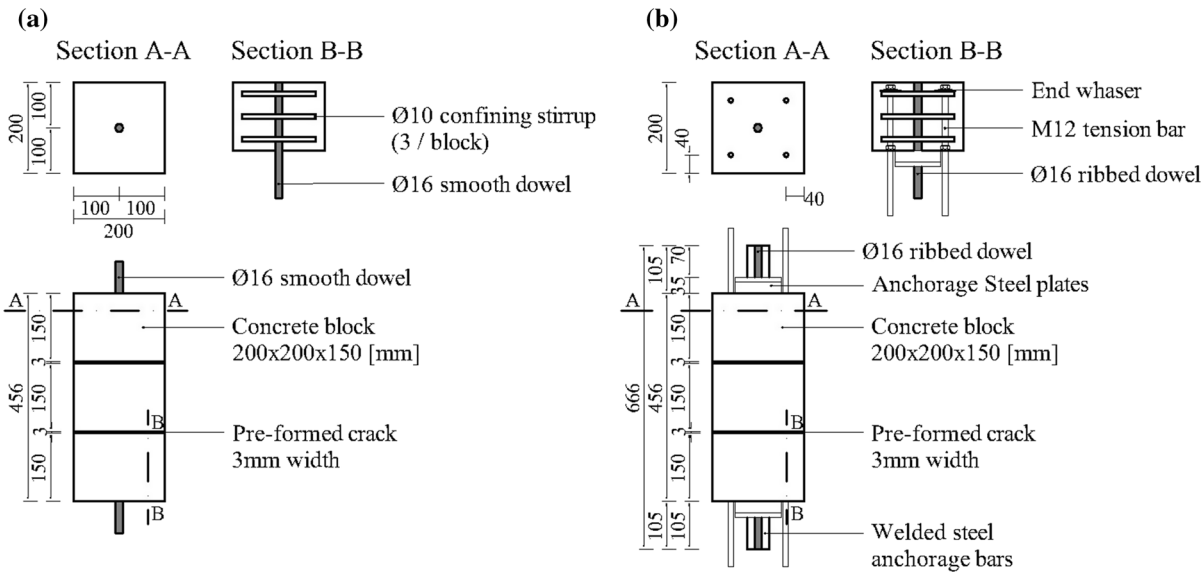

Fig. 1 Geometry of the specimens and details about the end anchorage system for smooth (**a**) and ribbed (**b**) dowel specimens (dimensions in [mm])

dowel and in contact with the prism face, provided equilibrium to the pull-out force in excess of the bond transfer capacity of the dowel embedded length, avoiding the pull-out failure. As for the cross section of the concrete blocks, it was proportioned sufficiently large to prevent possible concrete splitting failure, whose investigation is out of the scope of this study. In addition, three 10 mm diameter closed B450C stirrups were adopted to confine each concrete block and allow for a safety margin against splitting. The gaps separating the concrete blocks of each specimen had a width of 3 mm each, obtained introducing a plexiglass sheet during the cast process, then removed before the test execution to leave the desired target gap. The meaning of this gap is to inhibit any aggregate interlocking and friction shear mechanism between the concrete prism and to allow quantifying the pure dowel mechanism resistance, as it may develop in a widely open crack where sliding occurs.

The dowel rebar crossed all the blocks at their centreline. Diameter 16 mm smooth and ribbed dowels were tested; commercial hot rolled S275 JR steel [27] was adopted for the smooth bar dowels (P1 and P2 specimens), while a class B450C steel [24] is used for the ribbed ones (D specimens). Mechanical properties obtained from standard tensile tests [28], on specimens cut from the same bars of the smooth and ribbed dowel, measured 329 and 490 MPa yielding stress (f_y), 538 and 658 MPa ultimate stress (f_u), 19.9% and 10.2% maximum elongation (A_{10}), respectively. It is worth noting that the two types of steel are strongly different in term of yielding stress. This must be considered in the smooth and ribbed dowel result comparison. A total number of 12 samples of smooth bar dowel and other 8 specimens of ribbed bar dowel were tested. The concrete mix design was based on 340 kg/m^3 Portland cement CEM I 42.5R [29] dosage and a water/cement ratio equal to 0.55; standard three aggregate sizes to match the Bolomey curve [30] and no admixtures were adopted in the mix. All the specimens were realized in three series (P1, P2, and D) corresponding to three different castings. The mean compressive cylindrical strength and Young modulus of the three series measured about 34 MPa (34.03, 33.35, 33.66; CoV 4.20%, 5.84%, 2.83%) and 30GPa (27.64, 31.45, 28.65; CoV 7.7%, 11.8%, 7.3%), respectively, according to standard procedures [31, 32].

The axial load was applied in force control and kept constant during the shear cyclic loading applied to the dowel.

The shear load was applied by imposing a sliding between the central and the two end blocks. The loading frame is represented in Fig. 2.

A single jack pushed on the central block, reacting on a steel plate connected on the outer blocks by means of four couples of trusses working in tension and aligned with the specimen sliding planes at the preformed crack location. The load was transferred to each concrete prism by a couple of steel plates lightly tightened on the prism by four 12 mm threaded bars and pinned to the trusses. Shear load reversals were applied with a symmetric frame mounted on the specimen opposite side. The jack force was equally divided on the two shear planes by equilibrium. The symmetry of the specimen helps to avoid rotation due to possible eccentricities, which was monitored by dedicated gauges.

2.2 Instrumentation

The axial load was kept constant by a feedback control system. The shear load was applied by a hydraulic jack and red by a load cell placed between the actuator and the reaction frame (Fig. 2).

Vertical and horizontal relative displacements between the prisms were measured by potentiometric transducers. A schematization of their position is shown in Fig. 3. Four horizontal instruments (S-type) red the relative sliding between the central and the end concrete blocks: two gauges were placed parallel to the load application plane across each crack. The sliding on each shear plane is quantified as the average of the values measured by the two instruments reading on the same crack, thus compensating the concrete prisms relative rotation around the central rebar. Four vertical transducers (V-Type) are placed across each crack, on the block lateral faces. Their position is chosen for monitoring the relative rotations around the two principal horizontal axes; the mean crack opening is obtained by average. At the same time, each transducer could signal the possible contact between the crack sides, alerting for a possible shear transfer by friction. Finally, two other transducers measured the relative longitudinal displacement of the outer blocks, allowing a control of the total vertical deformation.

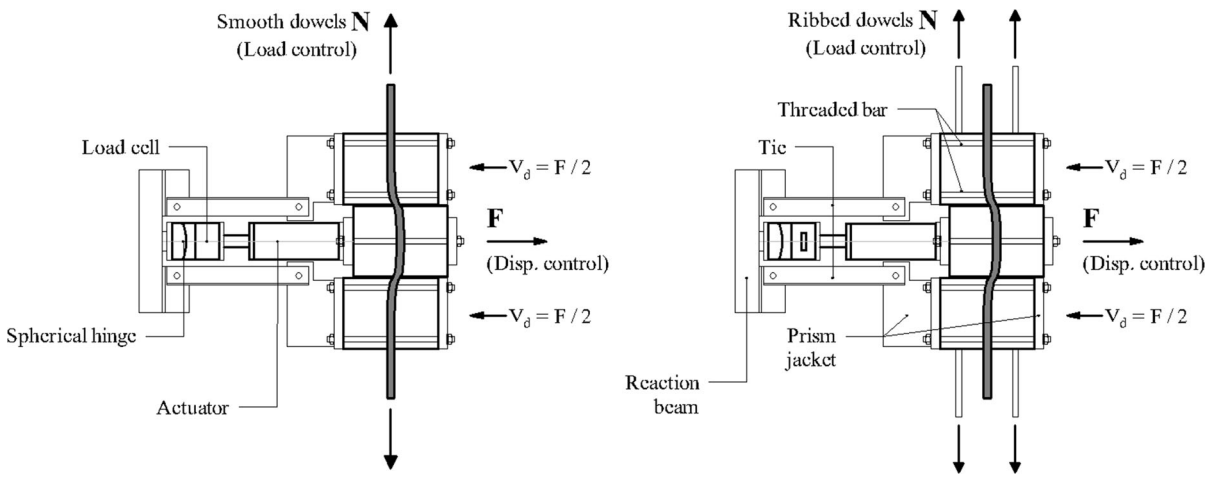

Fig. 2 Test set-up. Description of the two different options adopted for the application of the axial load (*N*) to the dowel specimens, in the case of smooth and ribbed rebar dowels. Description of the loading frame for the application of the shear action to the rebar dowel

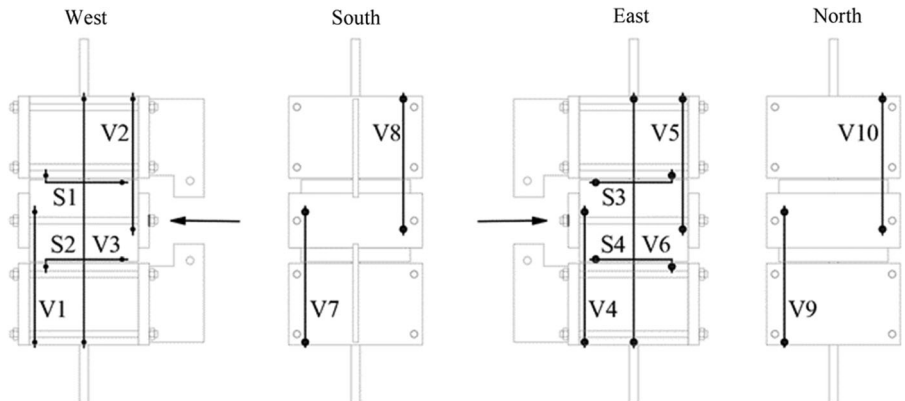

Fig. 3 Layout of gauges measuring the concrete block horizontal (*S*) and vertical (*V*) relative displacement

2.3 Load patterns

A series of cyclic shear test were conducted with different levels of axial load applied to the bar dowel (Table 1). Tests were conducted without axial load (N00) and others with a constant tensile force equal to three different percentages (N60, 90 and 98%) of the bar axial yielding strength. One sided cyclic shear loading was applied to the "*N*" series specimens, while only three specimens, named "NR", were subject to two-sided full cyclic shear loading.

The expected dowel yielding shear force V_{yd} was in first analysis evaluated through an analytical formulation adapted from literature (Eq. 1). The axial load effect on the dowel resistance is quantified through a coefficient $(1 - \alpha^2)$, where α is the dowel axial load normalized over the rebar yielding strength. This approach was proposed by Vintzēleou and Tassios, [33] (Eq. 2), after [34] and [13], neglecting the effect of the crack opening. Here the approach is implemented into the formulation proposed by Gelfi and Giuriani [20], which accounts for the load eccentricity due to the crack opening. The rearrangement of the proposal by Gelfi and Giuriani is reported in Eq. 1 and better explained in a dedicated paragraph in the following.

$$V_{yd}(N) = d_b f_{cc}\left(-a + \sqrt{a^2 + \frac{d_b^2 f_y(1-\alpha^2)}{3f_{cc}}}\right) \quad (1)$$

$$V_{yd}(N) = 1,3 d_b^2 \sqrt{f_y f_c (1-\alpha^2)} \quad (2)$$

Table 1 Nomenclature, axial force applied during the test and predicted shear yielding strength of each single specimen of smooth and ribbed bar dowels

Test	Samples	N/N_y (N_y) (%)	N [kN]	V_{yd} [kN]
N00	P1-1 P1-4 P2-1	0	0	31.1
	D-1 D-4			38.8
N60	P1-2 P1-5	+ 60	+ 40	24.2
	D-2 D-7		+ 65	30.3
N90	P1-3 P1-6	+ 90	+ 60	11.7
	D-3 D-8		+ 97	15.0
N98	P2-2 P2-3	+ 98	+ 95	4.0
	D-5 D-9		+ 105	5.3
NR00	P1-7	0	0	31.1
NR60	P1-8	+ 60	+ 40	24.2
NR90	P1-9	+ 90	+ 60	11.7

where N is the applied axial load, d_b the bar diameter, f_y the bar yielding stress; f_{cc} concrete bearing strength assumed equal to five times the concrete compressive strength f_c, $2a$ is the crack opening at the sliding plane.

The shear action is imposed to the samples by a gradual increase in amplitude. Generally, initial set-up cycles were performed with a force demand lower than the 15% of the predicted yielding shear one. Then, single cycles (typically two) at increasing fractions of the predicted yielding capacity were imposed. Finally, few cycles were performed to explore the plastic response of the system, reaching large deformation (at least 16 mm equal to the rebar dowel diameter) and high ductility levels. The complete presented history is followed for one sided cyclic shear tests; for the cycles with shear reversals, given the severe loading for the bar, the reference yielding load were imposed right after a preliminary cycle at reduced load (15% of the reference one). The loading protocol was adopted for each target axial load values N.

3 Experimental results

The test results are here described in terms of dowel shear action versus interface sliding curves. By symmetry of the specimen layout the dowel action, V_d, is assumed equal to half of the jack load. The sliding, s, of each dowel is quantified taking the average of the reading of the horizontal transducer placed on each specimen preformed crack. With reference to the instruments shown in Fig. 3, the sliding on the upper and lower sliding plane are quantified as:

$$s_u = (S1 + S3)/2 \tag{3}$$

$$s_l = (S2 + S4)/2 \tag{4}$$

According to [12, 13, 20], at the dowel mechanism yielding, two plastic hinges forms at each side of each single crack, causing a stiffness drop in the force–displacement response. The experimental yielding is reached on the two cracks at a different time, due to their inherent small differences. Then, the plastic deformation demand concentrates of on the first yielded shear plane (critical section). The following figures describes the dowel force versus the displacement measured on the critical section. The experimental cyclic responses are enveloped by a backbone curve, to help the comparison of the different specimen responses. A mean envelope curve is then highlighted to compare the behaviour of specimens tested under the different axial stress. Further details can be found in [35, 36].

The reading of the vertical potentiometric transducers was monitored to identify possible significant eccentricities, which can reflect in rotation on the vertical plane affecting the experimental response. Furthermore, a-posteriori check of the crack opening excluded any contact and consequent shear load transfer by friction or aggregate interlock, between the crack sides of the two blocks. No splitting cracks or anchor pull-out failure was observed in any tested specimen. This is the result of the specific proportioning and detailing of the test specimens, which in fact inhibited them. The discussion of such important mechanisms and their effect on the dowel response is out of the scope of this paper.

3.1 Dowel shear-sliding response

An example of cyclic dowel shear-sliding (V_d-s) curves is reported in Fig. 4, for the smooth rebar specimens with no axial load applied. A pre-yielding phase is observed with no significant residual displacement, whereas high plastic displacements were visible at large sliding amplitude. The non-linear shape of the force–displacement behaviour does not

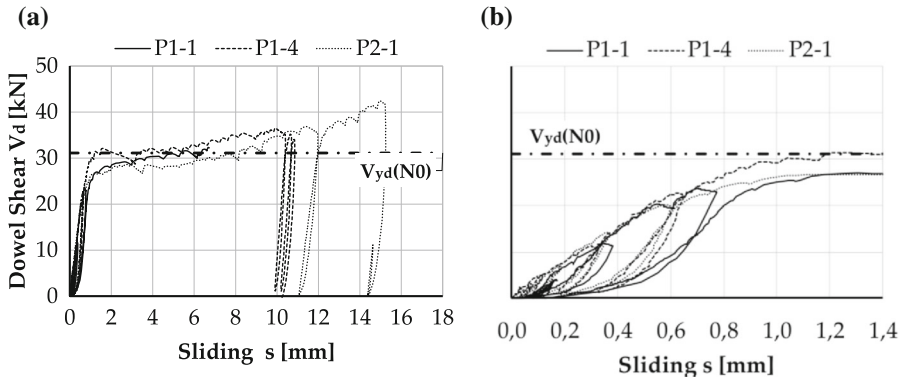

Fig. 4 Example of dowel shear load versus sliding curves for the smooth rebar tested without axial stress, measured at the critical section: complete response (**a**) and focus on the sliding displacement in the pre-yielding response (**b**)

allow for a clear identification of a specific yielding point; however, a markedly bi-linear response can be recognized.

In the following, only the backbone curves of the cyclic responses are reported. For each specimen, a grey line is plotted (Figs. 5, 6); then, a mean black bold curve is obtained for each axial stress level. The tests were pushed up to a target sliding equal to the dowel diameter. For some specimen the reported results end earlier due to the reaching of gauges end of stroke or the arising of specimen non-negligible unalignment because of the non-symmetric deformation of the two sliding sections (upper and lower preformed crack). All the dowel specimens showed a ductile response with a trend of hardening without failure, in the range of sliding displacement applied.

For the specimens with no axial load an average yielding strength of about 28 kN and 41 kN was obtained, in the case of smooth and ribbed dowels, respectively; the yielding point can be identified at

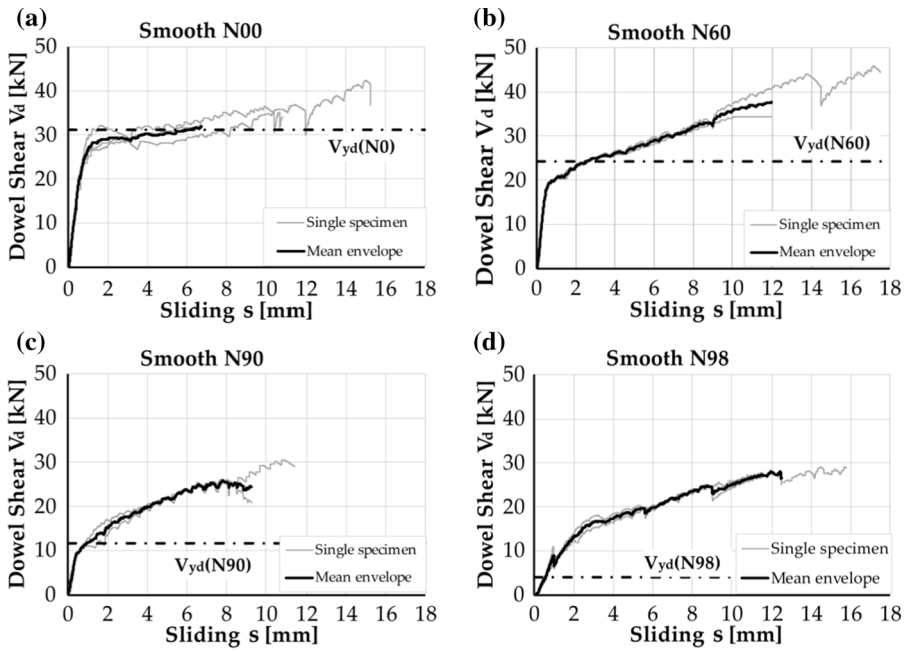

Fig. 5 Dowel shear force versus sliding response for smooth rebar specimens with different level of dowel axial load normalized on the rebar axial yielding strength (0%, 60%, 90% and 98%) and comparison with the prediction of dowel yielding shear strength $V_{yd}(N)$ according to Eq. 1

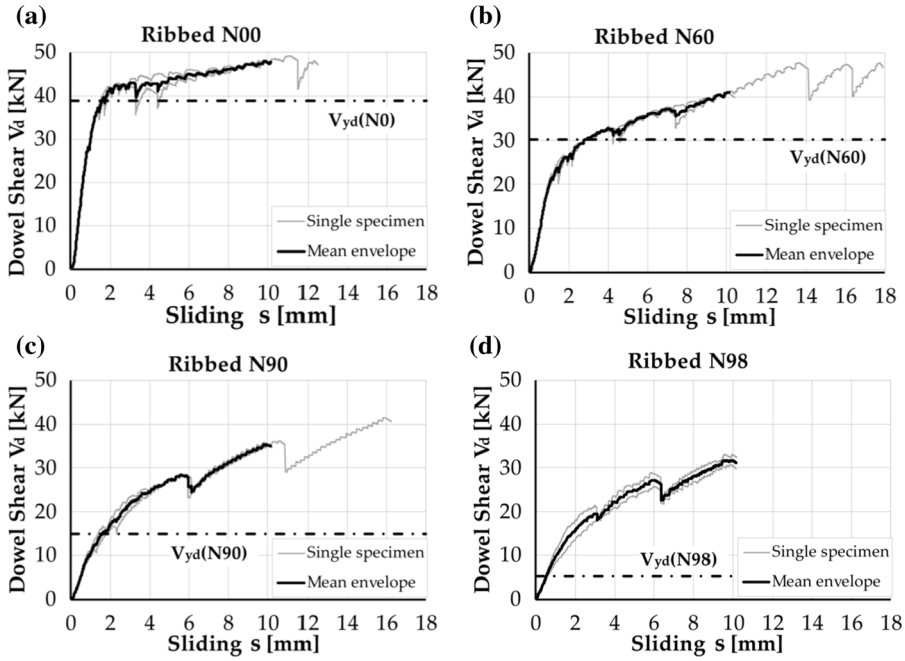

Fig. 6 Dowel shear force versus sliding response for ribbed rebar specimens with different level of dowel axial load normalized on the rebar axial yielding strength (0%, 60%, 90% and 98%) and comparison with the prediction of dowel yielding shear strength $V_{yd}(N)$ according to Eq. 2

about 1.20 mm and 2.00 mm. In the plastic field a constant strength can be considered up to 5.00 mm of displacement demand, followed by a little hardening behaviour. It is worth nothing that the results on smooth and ribbed bar dowels are not directly comparable to each other due to the difference in the rebar yielding stress capacity (329 and 490 MPa, respectively).

The introduction of the axial stress in the rebar significantly modified the dowel response: a drop in the yielding shear is evident, together with an increase of post-elastic stiffness. For the test N60 and N90, the mechanism yielding strength can be quantified in about 20 kN and 10 kN for the smooth bar dowel and in 25 kN and 15 kN for the ribbed one, respectively. The application of an axial load close to the bar yielding force (N98) significantly reduced the initial stiffness. Since the elastic stiffness remained basically the same for axial load values up to 90% of axial yielding, the drop of initial stiffness observed in the N98 specimens, suggests that the yielding mechanism was activated practically from the first load application, with a consequent shear yielding strength close to zero. A non-negligible residual dowel stiffness was obtained anyhow, ascribable to the kinking mechanism, as discussed in the following. In general, a smoother transition from the pre to the post yielding phase was observed for the ribbed bar, consistent with the observation of a higher local damage of the concrete around the bar at about the sliding plane.

Figure 7 reports the history of gap opening increase, $\Delta lgap$, as a function of the sliding, *s,* at the critical section. Figure 7a describes the response of one smooth and one ribbed dowel specimens under two different axial load conditions, namely 0% and 90% of the rebar axial yielding strength (N00 and N90). Focus is on loading cycles reaching 10 mm sliding amplitude. Figure 7b focus on cycles up to 5 mm sliding amplitude, describing the response of one specimen for all the four axial load conditions. The results show a trend of gap increase for all levels of axial load, which markedly increases with the axial load intensity. The rate of gap increase was higher for smooth dowel than ribbed one. A trend of gap increase under the application of cycles of sliding is clearly visible, more and more pronounced with the axial load increase. A sudden gap opening increase occurred at the application of the axial load followed by a linear trend with the sliding amplitude. A shift of increment induced unloading and reloading during cycles is

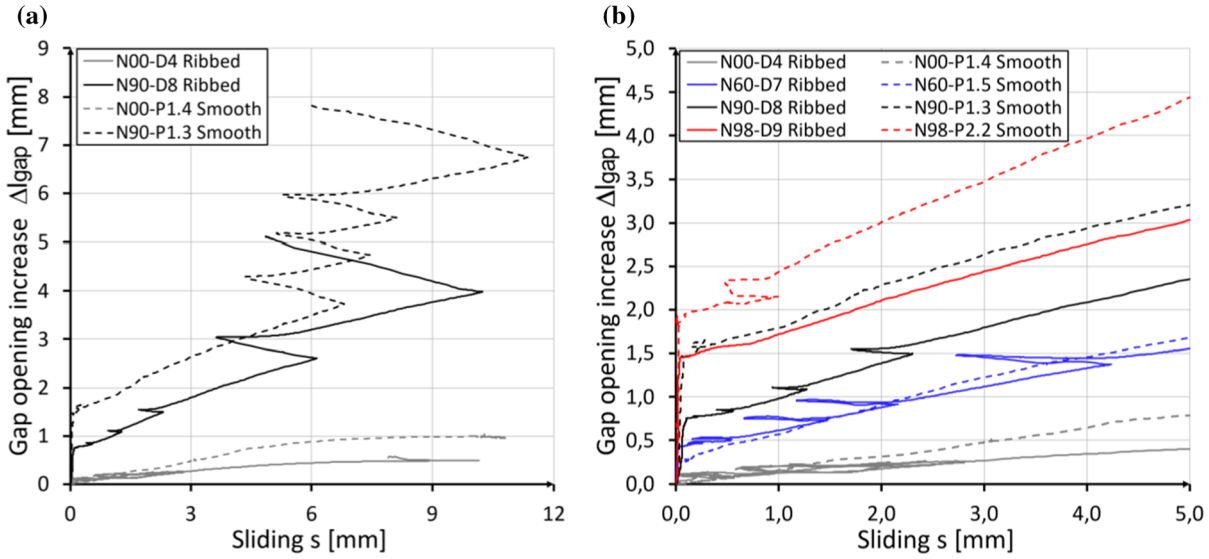

Fig. 7 Comparison of the measured gap opening increase versus dowel sliding at the critical section, for smooth and deformed dowel specimens. Example of the gap opening increase in subsequent cycles up to 10 mm sliding amplitude for selected specimens of two axial load conditions (N00 and N90) a); detail of the gap opening increase in a range of sliding up to 5 mm, for one specimen per all the four axial load conditions tested

clearly visible, more pronounced larger axial load conditions.

3.2 Response under cyclic shear reversals

Three specimens with smooth bar dowel were tested under cyclic shear with load reversals (8). They were characterized by three levels of axial load from zero to 90% of the rebar yielding strength, named NR0, NR60 and NR90. The shear-load response of P1-7 specimen showed symmetry; nevertheless, the cyclic response was significantly affected by pinching. This well-known phenomenon in dowels is related to the concrete plastic deformation and local damage under rebar local pressure [37]. Nonetheless, loading at a fixed deformation level, the same hysteresis loops were observed; thus, little in-cycle stiffness and strength degradation was observed. The unloading stiffness was nearly constant during all the tests. No relevant residual deformations were visible in the pre-yielding field.

In presence of axial load, the control of the specimen response after the reach of the yielding becomes more complex. With a normalized axial stress equal to 60% of the yielding, the shear cyclic response up to yielding point was symmetric without strength degradation. With higher axial stress (NR-90), the control of the shear-sliding behaviour was very difficult. Nonetheless, the detrimental effect of the axial load in the reduction of the dowel mechanism strength was newly confirmed, so as the hardening trend by increasing the imposed sliding (kinking mechanism), due to the tensile axial load in the dowel (Fig. 8).

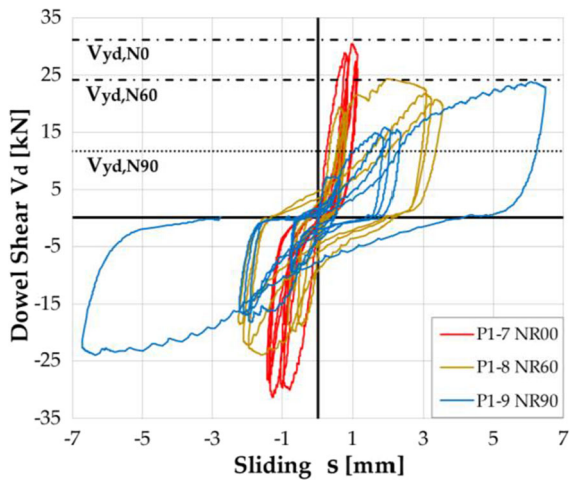

Fig. 8 Cyclic response of smooth bar dowel specimens P1-7,8,9 under repeated shear reversals at constant normalized axial stress levels of zero, 60 and 90% of the rebar yielding stress

4 Analytical modelling of the dowel response

An analytical modelling of the dowel behaviour is here proposed, to be applied under the condition that a splitting failure is prevented by adequate confinement. The aim of the model is to interpret the experimental results and allow for the dowel response prediction in presence of axial load. The prediction splits the dowel response in two, the pre-yielding and post-yielding phase. First, the dowel mechanism yielding strength is defined and quantified referring to the triggering of the full plastic flexural strength of the dowel cross-section. Then the dowel pre-yielding stiffness is quantified based on an elastic beam on elastic foundation (EBEF) approach. Finally, the kinking effect in presence of the applied axial load on the ribbed dowel is accounted for to quantify the dowel post-yielding stiffness. The approaches are taken from literature and adapted for a more comprehensive representation of the dowel response.

4.1 Dowel mechanism yielding strength

As for the dowel yielding strength, the formulation proposed by Gelfi and Giuriani [20, 26] is chosen and adapted to take into account the effect of the axial load on the rebar dowel response. Under the condition that the splitting failure is prevented, a ductile mechanism governed by flexure is identified in the rebar. Figure 9 describes the self-balanced static scheme assumed in the formulation. The limit-analysis approach is adopted, and the simplification includes both a plastic concrete bearing reaction and a plastic steel reinforcement response under flexure after yielding; thus the transition from first to full cross-section yielding and the rebar strain hardening are neglected (Fig. 10).

Given the symmetry of the dowel layout with respect to the sliding plane at the crack interface, the model assumes that a plastic hinge forms on each crack side at a distance L_{eff} from the point of contraflexure in the rebar. By imposing the equilibrium condition, it derives:

$$V_{\text{yd}} = d_{\text{b}} f_{\text{cc}} L_{\text{eff}} \tag{5}$$

$$M_{\text{y}}(N_{\text{s}}) = V_{\text{yd}}\left(L_{\text{eff}} + a\right) - \frac{1}{2} d_{\text{b}} f_{\text{cc}} L_{\text{eff}}^2 \tag{6}$$

where V_{yd} is the dowel mechanism yielding strength provided by the rebar flexural capacity, d_{b} the bar diameter, f_{cc} the concrete bearing strength (here assumed equal to five times the concrete compressive strength [33, 37], f_{c}, independently of the state of confinement), a the load eccentricity (assumed equal to half the crack width by symmetry), and $M_{\text{y}}(N_{\text{s}})$ the bar plastic bending moment strength related the actual axial load. By rearranging Eqs. 5 and 6, the equilibrium Eq. 7 is derived:

$$\frac{1}{2} d_{\text{b}} f_{\text{cc}} L_{\text{eff}}^2 + d_{\text{b}} f_{\text{cc}} a L_{\text{eff}} - M_{\text{y}}(N_{\text{s}}) = 0 \tag{7}$$

The solution of Eq. 7 allows to determine the distance L_{eff}. Given the bar dowel circular section and assuming a stress block approach, the solution of Eq. 7 can be obtained after determining the area of the cross-

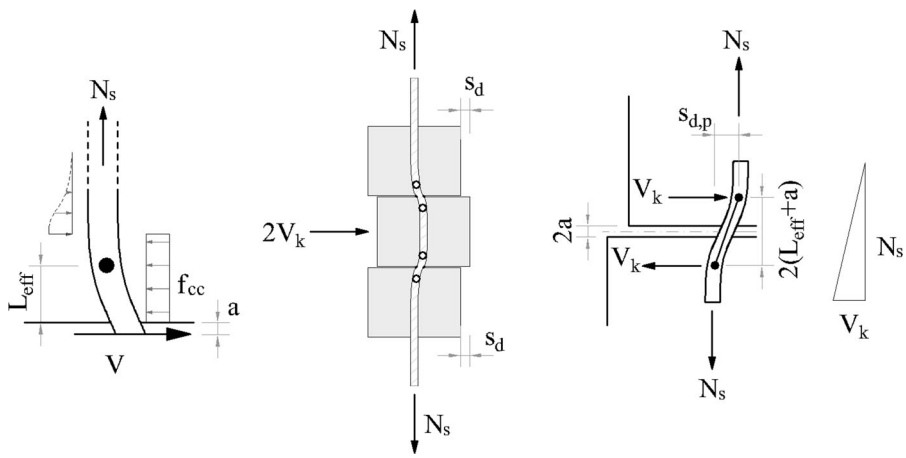

Fig. 9 Calculation scheme for the dowel mechanism yielding strength against sliding provided by the flexural rebar capacity (**a**) and for the kinking effect providing a re-centring reaction given by the axial load applied to the bar dowel (**b**)

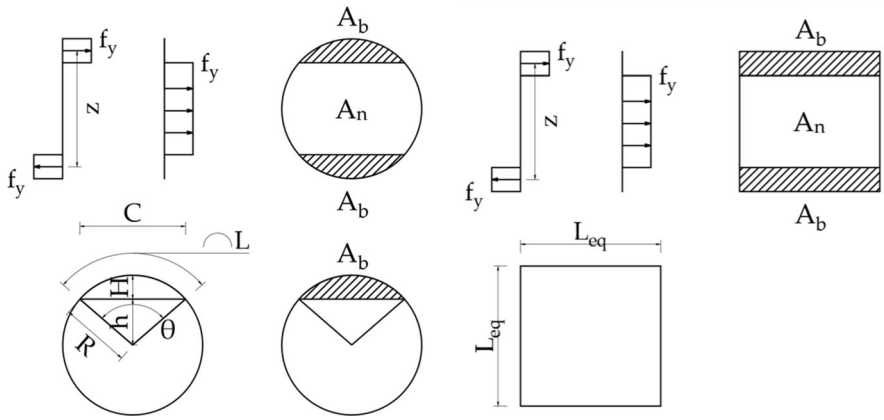

Fig. 10 Schematic of the section analysis assuming a stress block approach on the bar circular section and on the equivalent square one. A_b and A_n describe the area of the section giving equilibrium to the applied bending moment and axial load, respectively

section A_n required to balance the applied axial load and the geometry of the residual cross-section segments A_b (10.a), thus providing the bending moment capacity [37]. In order to simplify the approach, an equivalent square cross-section of side length L_{eq} can be defined, with the same area of the dowel circular cross-section, as represented in 10.b and according to Eq. 8:

$$L_{eq} = \sqrt{\pi d_b^2/4} \tag{8}$$

Solving Eq. 7 with the equivalent square cross section, Eqs. 9 and 10 provide the distance L_{eff} and the dowel mechanism strength as a function of the applied axial load:

$$L_{eff}(N_s) = -a + \sqrt{a^2 + \frac{L_{eq}^3 f_y \left[1 - \left(\frac{\sigma_s}{f_y}\right)^2\right]}{2 d_b f_{cc}}} \tag{9}$$

$$V_{yd}(N_s) = d_b f_{cc} L_{eff}(N_s) \tag{10}$$

The comparison of the results of the analytical prediction of the dowel mechanism yielding strength obtained with the circular and the equivalent square cross sections is reported in the dominion of Fig. 11 (paragraph 6) and shows a good approximation.

4.2 Dowel pre-yielding

The same literature proposal above recalled [20] is here adapted for modelling the dowel pre-yielding response. Assuming to subdivide the concrete volume surrounding the bar into independent slices parallel to each other and transverse to the bar axis, the concrete reaction can be assumed as that of a series of parallel plates subjected to a local in plane loading. According to the EBEF approach, the applied force V_i and the consequent deflection, δ_i, [38] are related by the stiffness K_c, quantified by Eq. 11.

$$K_c = V_i/\delta_i = \frac{\sigma_{ci} d_b}{(\sigma_{ci} d_b \beta / E_c)} = E_c/\beta \tag{11}$$

where the applied load on each slice V_i is balanced by the concrete uniform stress σ_{ci} on the rebar diameter d_b, E_c is the concrete modulus of elasticity and β is a coefficient dependent on the rebar spacing:

$$\beta = 2.5 \div 3.3 \tag{12}$$

The dowel elastic stiffness is defined by the following equations, based on the recalled analytical modelling approach [20]. The original formulation is here adapted to account for the load eccentricity, a, and the axial load, N, applied on the dowel:

$$s = \frac{V_d}{\lambda^2 E_s J_b}\left[\left(\frac{1 + a\lambda}{\lambda}\right) + a(1 + 2a\lambda)\right] \tag{13}$$

$$\lambda = \frac{2}{d_b}\sqrt[4]{\frac{1}{n\pi\beta}} \tag{14}$$

$$K_0 = V_d/s \tag{15}$$

with $n = E_s/E_c$ ratio of the reinforcement steel and surrounding concrete moduli of elasticity and J_b is the dowel cross section moment of inertia. Since the dowel mechanism is strongly nonlinear, the above

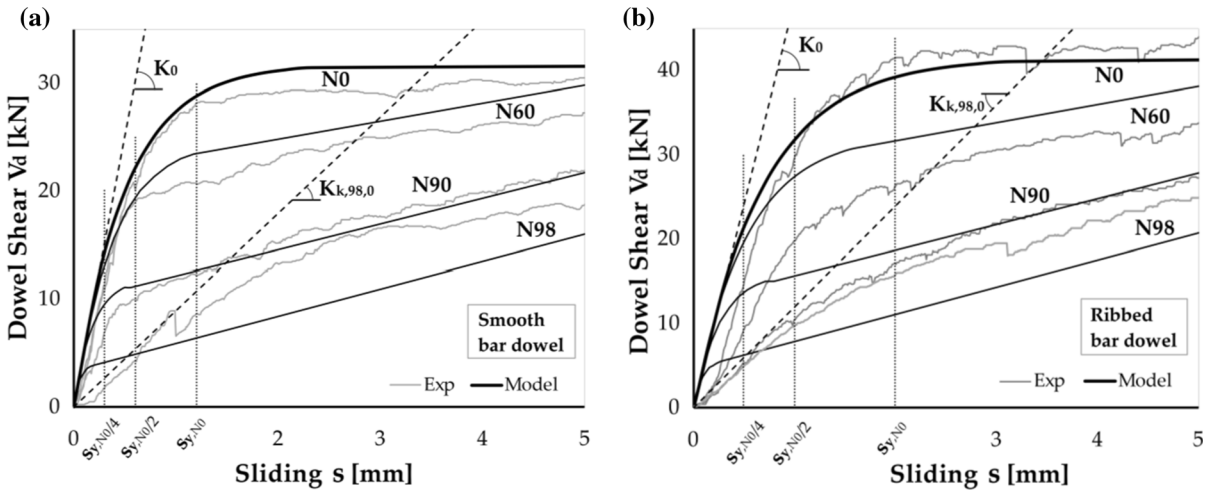

Fig. 11 Comparison between analytical prediction and the average backbone curve of the smooth (**a**) and ribbed (**b**) bar dowel experimental response for different values of applied axial load. The reported kinking stiffness $K_{k,98,0}$ assumes the effective length, $l_{eff,98}$, and the experimentally measured initial gap opening accounting for the application of the axial load equal to 98% of the rebar yielding strength. The model prediction continuous black curves propose a simplified kinking stiffnesses evaluated with constant gap opening (3 mm) and effective length, both calculated neglecting the effect of the axial load

defined value, K_0, describes only the initial tangent value of the dowel response. According to [20], the following dowel constitutive law is defined to account for the progressive reduction of the stiffness response with an asymptotic trend up to the yielding plateau:

$$V_d(N_s, s) = V_{yd}(N_s)\left(1 - e^{-K_0 s / V_{yd(N_s)}}\right) \quad (16)$$

The dowel mechanism yielding strength V_{yd} is here proposed with the direct formulation based on the equivalent square section, as previously presented, then accounting for the axial load applied to the bar dowel.

4.3 Dowel post-yielding stiffness

The tensile axial load applied on the dowel bar affects the post-elastic behaviour of the dowel mechanism offering a re-centring transversal reaction, known as kinking effect. With reference to Fig. 9, given the full exploitation of the rebar flexural strength in the dowel mechanism against sliding, in the post-yielding phase the rebar axial load at about the crack interface is inclined with component parallel to the sliding direction. The angle of inclination is here approximated with the angle of the straight line passing for the plastic hinges located at a distance L_{eff} from the faces, thus linearizing the dowel deformed shape. Accordingly, the post-yielding stiffness due to the kinking effect, K_k, is quantified by Eq. 17:

$$K_k = {}^{V_k}/_{s_{d,p}} = {}^{N_s}/_{2(l_{eff} + a)} \quad (17)$$

where V_k is the horizontal component of the rebar axial load in the point of contraflexure and $s_{d,p}$ is the horizontal distance between the plastic hinges. The effective value of L_{eff} end a are not easy to be determined in practical applications, as they vary with the progression of the dowel non-linear response. For the sake of simplicity, in the application of the proposed model in the design context, the plastic hinges distance from the point of contraflexure can be in first analysis assumed to be constant and equal to the effective length of the mechanism, $l_{eff,0}$, plus the load eccentricity, a_0, both evaluated in absence of axial load applied to the bar dowel (Fig. 11). Note that the reduction of L_{eff} when the dowel axial load increases is partly counterbalanced by the increase of crack opening due to the rebar elongation due to axial load and by the deepening of the plastic hinge as a consequence of the progressive concrete damage around the dowel, thus a compromise is accepted with the consequent approximation.

4.4 Test results versus analytical prediction

The comparison of the proposed model and experimental results is shown in Fig. 11, for the smooth and ribbed bar dowels. A value of $\beta = 3$ was adopted. The approach seems quite accurate in predicting the smooth bar dowel behaviour, with a limited strength overestimation; a more marked overestimation of the ribbed bar dowel initial stiffness response is observed for increasing values of axial load. This can be explained considering that the proposed model does not account for concrete damage in presence of the rebar slip, which is more significant for ribbed rebars, as observed in the discussion of the experimental results. Unfortunately, such damage can hardly be quantified, and a direct correlation seems feasible only by empirical calibration, as proposed for example in [16], but it is out of the scope of this paper. A further development of the method is thus required for the application to ribbed dowels. So far, the predicted resistance can be regarded as an upper bound for the ribbed dowel response. For axial load close to the rebar yield yielding (N98) the dowel response seems governed by the sole kinking effect. This observation is supported by the comparison, reported in Fig. 11, of the initial response of the N98 specimens with the initial stiffness of the kinking mechanism, $K_{k,98,0}$, evaluated according to Eq. 17. Such kinking stiffness is evaluated accounting for the effective gap opening measured after the application of the axial load for the specimens N98 (Fig. 7b) and the calculated effective length for the specific axial load level, according to Eq. 9. One may observe that for both smooth and deformed rebar, the calculated kinking stiffness, $K_{k,98,0}$, well approximates the initial dowel response stiffness. Then, increasing the sliding amplitude, the specimen response stiffness diminishes, implying a progressive increment of the distance between the dowel plastic hinges of the kinking mechanism (Fig. 9). This increment can be justified by the observed progressive increase of crack opening, the local damage arising in the concrete around the dowel and the rebar yield penetration inside the block. Unfortunately, except for the gap opening increase, the other parameters are not available to allow a quantification, so a simplified prediction is proposed in the comparison of Fig. 11.

5 Discussion of the results

5.1 Influence of the axial load

The experimental results show a trend of dowel yielding strength reduction by increasing the axial load, together with a post yielding stiffness increase.

The design of dowels should take into account such trend. Its interpretation is non-trivial as the markedly bilinear response of the dowel without axial load turns into a smoother curve as the axial load increases. Thus, the yielding threshold is difficult to be identified. Moreover, the kinking effect, increasing with the axial load, offers a resource of strength beyond the rebar yielding. The results show that the overall dowel stiffness diminishes by increasing the axial load, but a residual stiffness is anyhow ensured by the kinking effect. Such resource could be exploited in the safety verification, at the condition that the reduced stiffness and the consequent increased sliding demand does not jeopardize the rebar stability when subject to subsequent axial compression, as it typically happens for example in plastic hinges during seismic loading.

To help the understanding of the experimental results and appreciate the capabilities of the proposed model, Figs. 12 and 13 describe the role of the axial load and gap opening in the dowel response according to the analytical formulation proposed. Figure 12 shows the plots of the experimental dowel resistance measured at selected sliding amplitudes as a function of the dowel axial load and compares them with the prediction of dowel yielding strength obtained from Eqs. 9 and 10. The comparison is drawn for both smooth and ribbed dowels. The reference sliding values selected correspond to the sliding at the nominal experimental yielding, $s_{y,N0,}$ assessed at the beginning of the post-yielding branch in the backbone curves of the specimens without axial load (1,2 and 2 mm for the smooth and ribbed bar dowels, respectively), as highlighted in Fig. 11. One half and one quarter values are also considered to qualitatively interpret the observed trend of reduction of the sliding amplitude at yielding with the increase of axial load in the dowel specimens. Figure 12 compares also the dowel yielding prediction with the Elastic beam on elastic foundation approach, based on the yielding surface criterion, as proposed by Maekawa and Qureshi [16]. In the comparison is reported also the dowel resistance obtained with Eq. 18, adopted by the

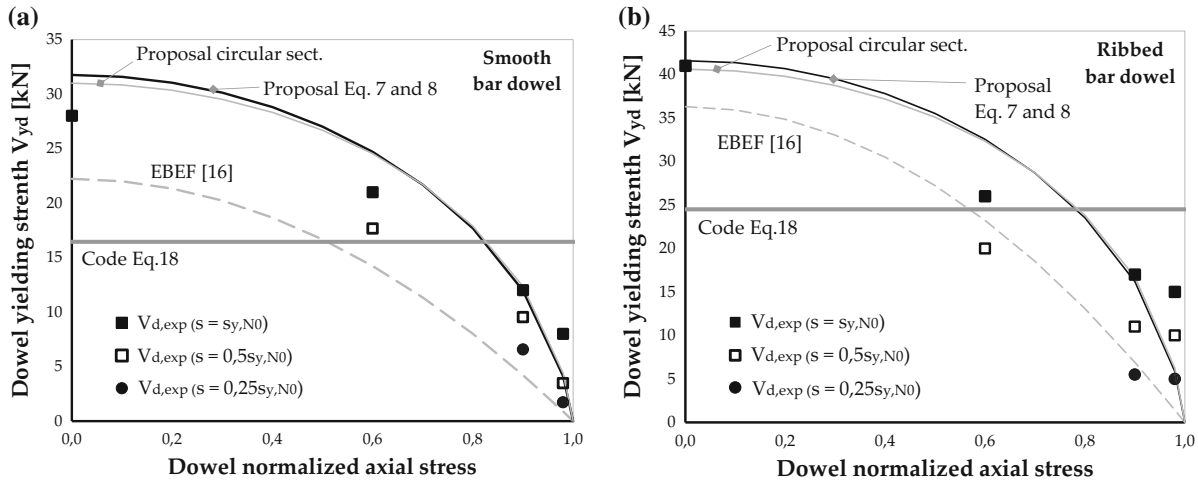

Fig. 12 Comparison of the theoretical and experimental shear dowel yielding strength versus bar axial load dominion for the smooth (**a**) and ribbed (**b**) bar dowels

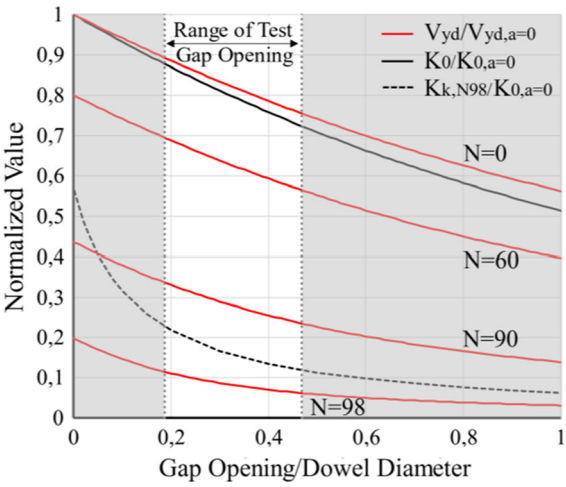

Fig. 13 Trend of variation of the calculated dowel shear yielding strength, initial stiffness and kinking stiffness as a function of the gap opening, for specific values of axial load applied to the dowel rebar (according to Eqs. 9, 10, 15, 17, respectively). The highlighted range of test gap opening corresponds to cycles of shear loading up to 5 mm sliding amplitude

Italian [24] and the European [25] codes to account for the rebar dowel contribution in the sliding verification at the base of RC shear walls.

$$V_{\mathrm{d}} = 0,25 A_s f_{\mathrm{yd}} \tag{18}$$

where A_s is the bar dowel cross section area and f_{yd} is the rebar design tensile yielding stress. To allow for the comparison with the experimental results, in Fig. 12 the shear strength obtained from Eq. 18 is quantified assuming the measured rebar specimen yielding stress instead of f_{yd}. The prediction of Eq. 18, applied to the single rebar dowel, appears safe sided only in presence of an axial stress lower than the 60% of the yielding one, for both smooth and ribbed dowel. Both the EBEF and the proposed approach well captures the trend of dowel strength reduction with the increase of axial load. The EBEF approach, neglecting the exploitation of the rebar full flexural capacity tends to underestimate the dowel capacity, especially for smooth rebar dowels. The proposed simplified approach on the contrary tends to slightly overestimate the dowel strength, probably due to the consideration of the rebar full flexural capacity, which may fully develop at displacements larger than the dowel yielding one, as shown in Fig. 11.

Figure 13 emphasizes the role of gap opening on the dowel response. The trend of variation of the initial stiffness, yielding strength and kinking stiffness as a function of the gap opening are reported. They are calculated according to Eqs. 9, 10, 15 and 17 respectively. In detail the initial and kinking stiffnesses are normalized to the initial stiffness evaluated for zero axial load and gap opening; similarly, the dowel yielding strength is normalized to the value calculated with no axial load and gap opening. The gap opening is normalized to the bar dowel diameter. The Figure reports also the range of gap opening measured in the test for sliding cycles up to 5 mm amplitude, consistently with Fig. 11. Note that the kinking

stiffness is calculated for an axial load equal to 98% of the rebar yielding strength to allow comparison with the results of Fig. 11. The residual stiffness against sliding offered by kinking, when the rebar is subject to axial load close to yielding, is non negligible but small compared to the stiffness of the dowel calculated neglecting the role of axial load. Such kinking effect decreases quickly with the gap opening, which is likely to occur when high tensile action applies to the dowel. The trend of stiffness and strength reduction reported in Fig. 13 is expected to further emphasize under the effect of the local concrete damage due to splitting or bar pull-out, which are neglected in the calculation.

5.2 Influence of the bar surface

No direct comparison between the responses of different bar surface roughness is possible since the smooth and the ribbed bar were characterized by significant different mechanical properties. However, some interesting differences can be observed.

With reference to Fig. 11, without axial load, the initial elastic branch of the force–displacement relationships is similar for both the plain and the ribbed rebar. By increasing the axial stress, a decrease of the ribbed rebar response stiffness can be observed. This can be explained by the observed damage of the concrete surrounding the bar caused by the ribs [16], which reduces the stiffness of the concrete bearing reaction in the dowel mechanism. In general, a stronger non-linear behaviour was observed for the ribbed bars than for the smooth ones; consequently, the yielding point identification is more difficult for this kind of dowel. Finally, the dowels axially loaded near to the yielding point (NT-98), for which the mechanism is mainly governed by the kinking effect, showed a similar initial stiffness normalized to the rebar axial yielding strength. Such stiffness resulted slightly larger for the smooth rebar than for ribbed ones, suggesting larger kinking distances for the latter dowel type, despite of a larger crack opening measured for the smooth rebars. This results further suggest a higher local damage in the concrete surrounding the dowel for rebars with ribbed surface.

6 Conclusions

Based on the results of the presented experimental campaign, the dowel resistance offered by a rebar crossing an orthogonal crack is strongly dependent on the axial stress applied on the same rebar. By increasing the axial load acting in the dowel, both the stiffness and yielding shear strength of the mechanism decreases. A significant hardening behaviour was observed in presence of a tensile action applied to the bar dowel, due to the so-called kinking effect, which was found to increase with the axial load magnitude. Cycle loading with shear reversals confirmed this trend. For axial load close to the rebar yielding strength, the kinking mechanism was found to ensure a certain residual stiffness of the dowel against shear action, that progressively reduce by increasing the sliding amplitude and the crack opening.

An analytical based model to predict the dowel response in presence of axial load is proposed, adapting previous proposal from literature. The model can capture both the stiffness and strength capacities of smooth dowel in the elastic and plastic field as exhibited in the tests. It is based on limit-analysis for the definition of the yielding mechanism capacity and on the elastic beam on elastic foundation approach for the prediction of dowel stiffness. A certain overestimation of the elastic stiffness and shear strength characterizes the prediction of ribbed dowel shear-sliding behaviour probably due to the damage of the concrete surrounding the dowel due to the presence of the ribs, which is not accounted in the model present formulation. For axial load close to the rebar yielding strength, the model of the kinking mechanism can capture the dowel initial stiffness, under the condition of knowing the effective crack opening. When this information is not available, a simplified approach allows to obtain an acceptable estimate of the dowel response. The model formulation is suitable for hand calculation, and it can helpfully assist the design and verification of rebar dowel. Further studies are needed to quantify the effect of concrete damage due to ribbed rebar pull-out and to fully understand the dowel response under cyclic loading in presence of both axial and shear reversal.

Acknowledgements The authors gratefully acknowledge Fabrizio Pezzarossi, Luca Bonetti, Alberto Zucchetti and the

technicians of the P. Pisa Lab of the University of Brescia for their assistance in the experimental testing.

Funding Open access funding provided by Università degli Studi di Brescia within the CRUI-CARE Agreement.

Declarations

Conflict of interest The authors declare that they have no conflict of interest.

References

1. Hofbeck JA, Ibrahim IO, Mattock AH (1969) Shear transfer in reinfroced concrete. ACI J 66(13):119–128
2. Maekawa K, Qureshi J (1997) Stress transfer across interfaces in RC due to aggregrate interlock and dowel action. J Mater Conc Struct Pavements JSCE 557/V–34:159–172
3. Carvalho EC, Coelho E (1997) Numerical investigations on the seismic response of R.C. frames designed in accordance with Eurocode 8, ECOEST-PREC8 Rep. 7. Laboratorio Nacional de Engenharia Civil (LNEC), Lisbon
4. Riva P, Meda A, Giuriani E (2003) Cyclic behaviour of a full scale RC structural wall. Eng Struct 25:835–845
5. Fardis MN (2009) Seismic design, assessment and retrofitting of concrete buildings: based on EN-Eurocode 8. Springer. https://www.springer.com/gp/book/9781402098413. Accessed 02 Sept 2019
6. Preti M, Giuriani E (2011) Ductility of a structural wall with spread rebars tested in full scale. J Earthq Eng 15(8):1238–1259. https://doi.org/10.1080/13632469.2011.557139
7. Verderame GM, Fabbrocino G, Manfredi G (2008) Seismic response of RC columns with smooth reinforcement. Part I: monotonic tests. Eng Struct 30(9):2277–2288. https://doi.org/10.1016/j.engstruct.2008.01.025
8. Verderame GM, Fabbrocino G, Manfredi G (2008) Seismic response of RC columns with smooth reinforcement. Part II: cyclic tests. Eng Struct 30(9):2289–2300. https://doi.org/10.1016/j.engstruct.2008.01.024
9. Di Ludovico M, Verderame GM, Prota A, Manfredi G, Cosenza E (2014) Cyclic behavior of nonconforming full-scale RC columns. J Struct Eng 140(5):04013107. https://doi.org/10.1061/(ASCE)ST.1943-541X.0000891
10. Brenna A, Dei Poli S, Di Prisco M (1990) Dowel action: some experimental and theoretical results regarding special concretes (in Italian). Studi e Ricerche (5)
11. Dei Poli S, Di Prisco M, Gambarova PG (1992) Shear response, deformations, and subgrade stiffness of a dowel bar embedded in concrete. ACI Struct J 89:665–675
12. Dulacska H (1972) Dowel action of reinforcement crossing cracks in concrete. ACI J 69(12):754–757
13. Soroushian P, Obaseki K, Rojas MC, Jongsung S (1986) Analysis of dowel bars acting against concrete core. ACI J 83(4):642–649
14. Vintzēleou EN, Tassios TP (1987) Behavior of dowels under cyclic deformations. ACI Struct J 84(1):18–30
15. Walraven JC, Reinhardt HW (1981) Theory and experiment on the mechanical behaviour of cracks in plain and reinforced concrete subjected to shear loading. HERON J 26(11):25417
16. Maekawa K, Qureshi J (1996) Computational model for reinforcing bar embedded in concrete under combined axial pullout and transverse displacement. J Mater Conc Struct Pavements JSCE 538/V–31:227–239
17. Maekawa K, Qureshi J (1996) Embedded bar behavior in concrete under combined axial pullout and tansverse displacement. J Mater Conc Struct Pavements 5. 12/V-30:183–195
18. Soltani M, Maekawa K (2008) Path-dependent mechanical model for deformed reinforcing bars at RC interface under coupled cyclic shear and pullout tension. Eng Struct 30(4):1079–1091. https://doi.org/10.1016/j.engstruct.2007.06.013
19. Moradi AR, Soltani M, Tasnimi AA (2012) A simplified constitutive model for dowel action across RC cracks. ACT 10(8):264–277. https://doi.org/10.3151/jact.10.264
20. Gelfi P, Giuriani E (1987) Theoretical constitutive law for dowel connections (in Italian). Studi e Ricerche 9
21. Matsunaga K et al (2021) Modeling of dowel action for cast-in and post-installed anchors considering bond property. Eng Struct 245:1173
22. Verderame GM, Ricci P, Esposito M, Sansiviero FC (2001) Mechanical properties of reinforcement used for RC constructions from 1950 to 1980 (in Italian). In: 10th national conference "L'Ingegneria Sismica in Italia" 8
23. Feldman L, Bartlett M (2005) Bond strength variability in pullout specimens with plain reinforcement. ACI Struct J 102:860
24. Norme Tecniche per le Costruzioni (2018) Decreto Ministeriale 17 Gennaio 2018 - Norme Tecniche per le Costruzioni. Ministero delle Infrastrutture (in Italian)
25. Eurocode 8 (2004) Design of structures for earthquake resistance—part 1: general rules, seismic actions and rules for buildings. European Committee for Standardization, Brussels
26. Giuriani E (2012) Strengthening of historical buildings (in Italian). UTET
27. EN 10025 (2019) Hot rolled products of structural steels
28. UNI EN ISO 15630-1:2019 (2019) UNI EN ISO 15630-1:2019 Acciao per Calcestruzzo Armato e Calcestruzzo Armato precompresso - Metodi d prova - Parte 1: Barre, Rotoli e Fili per Calcestruzzo Armato

29. UNI EN 197-1:2011 (2011) UNI EN 197-1: Cemento - Parte 1: Composizione, specificazioni e criteri di confromità per cementi comuni
30. Bolomey J (1927) Bulletin. ASCE 16:22–24
31. UNI EN 12390-3 (2003) UNI EN 12390-3 testing hardened concrete—compressive strength of test specimens
32. UNI EN 12390-13 (2013) UNI EN 12390-13 testing hardened concrete—determination of secant modulus of elasticity in compression
33. Vintzēleou EN, Tassios TP (1986) Mathematical models for dowel action under monotonic and cyclic conditions. Mag Concr Res 38(134):13–22. https://doi.org/10.1680/macr.1986.38.134.13
34. Rasmussen BH (1963) The carrying capacity of transversely loaded bolts and dowels embedded in concrete. Bygningsstatiske Meddelser 34
35. Paderno A (2021) Seismic behaviour of existing RC frames in presence of plain reinforcement. Ph.D. thesis, DICATAM University of Brescia, Italy
36. Paderno A, Cominoli L, Bolis V, Preti M (2019) Studio sperimentale della resistenza a spinotto di barre lisce nel calcestruzzo sottoposte ad azione combinata di taglio-trazione. In: Proceedings of the XVIII Anidis conference "L'ingegneria sismica in Italia", Sept 15–19, 2019, Ascoli Piceno, Italy
37. Biolzi L, Giuriani E (1990) Bearing capacity of a bar under transversal loads. Mater Struct 23(6):449–456. https://doi.org/10.1007/BF02472028
38. Melan E (1925) Die verteilung der kraft in einem streifen von endlicher breite. Zschr F angew Math Mech, Band 5, Heft 4, Prag